

A Simple Energy Recovery Scheme to Harvest the Energy from Shaded Photovoltaic Modules During Partial Shading

Mohd. Zulkifli Ramli and Zainal Salam, *Member, IEEE*

Abstract—This paper proposes a simple circuit to recover the energy that otherwise would be lost due to the partial shadings on photovoltaic (PV) modules. Since the circuit can be readily retrofitted to an existing PV system, no modification on the central inverter is required. The main idea of the scheme is that, during partial shading, parts of the current from the nonshaded modules are harvested by an energy recovery circuit using power electronic switches and storage components. In doing so, the current of the PV string is maintained at the level generated by the shaded module. There is no need for the shaded module to be short-circuited; as a result, it can still actively produce output power (despite being partially shaded). To investigate the idea, the proposed circuit is retrofitted to a prototype PV system using eight modules. The partial shading conditions are emulated using a solar simulator with a controllable irradiance capability. The results are validated by a good agreement between the experimental and simulation works.

Index Terms—Energy recovery, inverter, maximum power point (MPP), maximum power point tracking (MPPT), partial shading, photovoltaic (PV).

I. INTRODUCTION

FOR many years, the central inverter has been the preferable choice for large as well as small photovoltaic (PV) system installations [1], [2]. In this configuration, a number of PV modules are connected in series to form a string. Several of these strings are arranged in parallel to form an array, which is then connected to one central inverter. This is known as series-parallel connection and is a typical setup for the PV power generation system. The merits of the PV system with central inverters are well known: simple installation, less maintenance, and high reliability [3], [4]. However, it does exhibit several disadvantages, one of which is the severe reduction in the throughput power when one or a number of modules are subjected to partial shading [1], [5]–[11]. In the building integrated

PV system, the shading normally originates from the nearby tree, building, chimney, power line poles, or similar objects. These factors may be unavoidable due to the building congestion in urban areas and unforeseen erection of new structures. In a large PV power generation system (PV farm), the partial shading can be caused by clouds that strike on certain spots of the solar array, while other parts are left uniformly irradiated. In certain cases, the remains of birds or animals cause the shading on the modules. Another source of partial shading-like characteristics is exhibited by module irregularities; a common example would be the presence of cracks on one or more modules of the PV array.

With the presence of partial shading, the behavior of the PV system becomes very complicated. This is because the shaded module acts as a load instead of a generator; consequently, a hot spot is created and if left unprotected, the module may experience irreparable damage. Typically, every module is connected to a bypass diode to divert the current in the case of partial shading occurrence. However, when the bypass diode is activated, the P - V characteristic curve exhibits multiple peaks, i.e. several local along with one global peak [5], [6], [12]–[15]. If the system is equipped with the conventional maximum power point tracking (MPPT) such as perturbed and observed (P&O), increment conductance or Hill-climbing, it would be very difficult to track the true maximum power point (MPP) peak because these algorithms could not discriminate between the local and the global peaks. In most cases, the MPPT will settle at a local peak, possibly resulting in a huge loss of power [1], [6], [16]–[18]. Furthermore, when the current flows through the bypass diode, conduction losses occur, further degrading the system's efficiency.

There are efforts using sophisticated MPPT schemes such as modified P&O [6], [19]–[22], particle swarm optimization [13], [20], [23], ant colony optimization [24] and the direct search method [25]. Despite the success of these algorithms to track the global peak [13], [23], [26], it must be noted that as long as the shaded module is being short-circuited by the bypass diode, it is totally unusable. However, the shading phenomena may not always be so severe such that the module receives zero irradiance. It is known that, depending on the severity of the shading, there is a certain amount of power that could possibly be captured by the shaded module. Despite this fact, the opportunity to harvest this power is lost due to the activation of the bypass diode.

Hence, various methods are devised to recover the power from the shaded module. One approach is to place a small

Manuscript received April 25, 2013; revised September 2, 2013 and December 1, 2013; accepted January 7, 2014. Date of publication January 24, 2014; date of current version August 13, 2014. This research was supported by the Ministry of Higher Education Malaysia, under the Research University Grant 2423.00 G40. The project is managed by the Research Management Centre, Universiti Teknologi Malaysia. Recommended for publication by Associate Editor V. Agarwal.

M. Z. Ramli is with the Faculty of Electrical Engineering, Universiti Teknikal Melaka, 76100 Melaka, Malaysia (e-mail: mohd.zulkifli@utem.edu.my).

Z. Salam is with the Centre for Electrical Energy Systems, Faculty of Electrical Engineering, Universiti Teknologi Malaysia, 81310 Johor Bahru, Malaysia. (e-mail: zainals@fke.utm.my).

Color versions of one or more of the figures in this paper are available online at <http://ieeexplore.ieee.org>.

Digital Object Identifier 10.1109/TPEL.2014.2302007

dedicated dc–dc converter to every module; then these modules are connected to the central inverter [5], [12], [26]–[28]. In the literature, this method is known as the distributed MPP configuration. The converter normally has a power rating approximately equal to the module itself and is equipped with its own MPPT controller. Using this scheme, the nonshaded modules are not affected by the shaded ones, and the power from the latter can be independently harvested. Although attractive, the method inhibits several shortcomings. During normal operation, the converter conducts the full load current, resulting in high conduction and switching losses [28]. Furthermore, the reliability of the electronic components is reduced due to their exposure to harsh environment conditions, particularly high operating temperature. This is unavoidable since the converter is mounted underneath the module itself [29], [30]. Alternatively, there are considerable efforts to develop the dc–ac converter for each module (known as microinverter), which is directly connected to the ac grid [3], [26], [27], [31]–[37]. Using the concept, the central inverter is not required because the microinverter has its own MPPT and inversion and voltage step-up mechanism.

Another method to utilize the power from the shaded modules is proposed by the authors in [38]. In this technique, a bidirectional buck–boost, flyback or Cuk converter is used to divert the current of the nonshaded modules by controlling the duty cycle of the converters. During partial shading, the energy from the nonshaded modules is transferred to the inverter and consumed by the PV system. The work in [30] only demonstrates the workability of the approach using two modules per converter. However, to accommodate more than two modules, the converters need to be overlapped to allow for the string current from the nonshaded module to be properly diverted. As a result, for every interconnection between a group of two modules, additional two switches and two diodes are required. A similar scheme, albeit using a different circuitry, has been proposed by Shimizu *et al* [14]. Despite its effectiveness, the main drawback of the scheme is the switching limitation; for example, for four modules in series, the off duty cycle range is limited to 25%. For higher number of modules, the off duty cycle is even lower. This is because within a single switching cycle, only one switch is forced to be turned OFF, while others remain ON. The limited off duty cycle restricts the ability of the circuit to control the power flow under severe shading condition. In addition, although the scheme utilizes MPPT to improve the efficiency of the circuit, the authors do not mention its performance during partial shading and how it is synchronized to the MPPT of the central inverter. There are also concerns regarding the accuracy of the voltage and current sensors (used for MPPT computation) when subjected to the high temperature beneath the modules.

In [39], an alternative method using a single inductor per four modules is proposed. Despite the reduced inductor, the circuit requires a large number of switches and diodes, i.e. for a four-module system, eight switches and ten diodes are needed. Furthermore, during the inductor charge and discharge cycles, only one combination of switches and diodes is switched ON and OFF; others are not active. Under this constraint, the best switching combinations have to be found in order to deliver the maximum power during partial shading. However, in many

cases, the search for the optimum switching configuration is complex and requires a substantial amount of time. Thus there are possibilities that the algorithm may not be able to cope with rapidly changing cloud condition. For example, as described in [25], the fluctuation in irradiation can go up to 15 times within 1 minute. If the partial shading occurred during this period, an efficient tracking could not be guaranteed. More recently, an energy recovery scheme for shaded module for the multilevel inverter is reported [40]. Despite its ability to harvest the power during partial shading, the buck converter always conducts at full load current during a normal condition. This causes high switching and conduction losses. Another drawback of this technique is the complexity of the switching due to the multilevel inverter structure.

With regard to these issues, this paper describes an attempt to improve the capabilities of the topologies described above. The proposed scheme is based on a group of four modules (one unit), but can be extended to accommodate a large number of modules by combining other units using a simple interconnecting circuits. The number of switches for four modules (one unit) is 1, and for the interconnection of two units, an additional two switches and one inductor are needed. The circuit is only active during the event of partial shading; during uniform irradiance, it is isolated from the PV system. Besides, the switching pattern for the switch is simple, i.e. it operates based on an opened-loop concept, using a fixed 50% duty cycle. Consequently, the scheme can be implemented using a low cost digital circuit, which is much simpler than the closed-loop system proposed by the authors of [12] and [30]. The latter requires microcontrollers, current, and voltage sensors for MPPT computation. In average, the circuit utilizes 0.5 inductor per module, compared to one per module for topologies in [12], [14], and [38]. Since the circuit is readily retrofitted to the PV system, no modification into the existing central inverter is required. It can be plugged under the module with minimal additional wirings.

It has to be noted that the idea and concept of this topology was initially published in [8]. However, in that paper, there is insufficient detail on the analysis of the circuit operation. Furthermore, limited results are presented, i.e. the circuit performance is illustrated by only four modules, which implies that the interconnection circuit between the different units is untested. In this paper, an extensive analysis is carried out to describe the operation of the energy recovery circuit from shaded modules. An experimental test rig involving eight (retrofitted) PV modules, along with an in-house solar simulator, is constructed. Using the solar simulator, various partial shading conditions are emulated to verify the performance of the proposed circuit. The efficiency of the proposed work is evaluated against the typical PV system (i.e. with the bypass diode only). It is envisaged that the improvements mentioned previously yield a satisfactory return of investment over the long run.

II. PROPOSED CIRCUIT

A. General Block Diagram

Fig. 1 shows the overall block diagram of the proposed circuit to harvest the power from the shaded module. The circuit

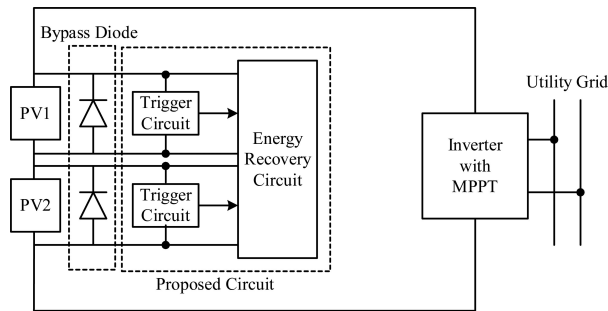


Fig. 1 Overall block diagram of the proposed PV power generation system retrofitted to a grid-connected PV.

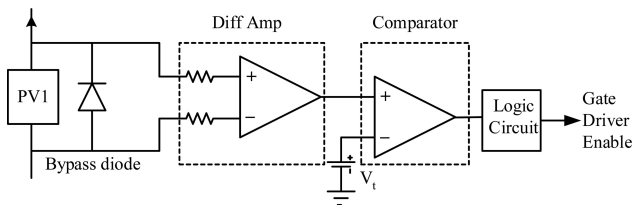


Fig. 2 Trigger circuit.

is connected in parallel to the original PV modules; therefore, it can be easily retrofitted to the existing system with minimum changes in the electrical wirings. In Fig. 1, the PV system is a grid-connected type using one central inverter with MPPT. However, the proposed circuit can be equally effective for stand-alone system, for example, using battery banks. Note that the circuit only functions during the occurrence of partial shading. Under the uniform irradiance, the PV system operates in the normal way, i.e. the bypass diode is in the OFF state. During this condition, the circuit draws minimal power, just enough to maintain the operation of the trigger circuit.

When partial shading occurs, the trigger circuit is automatically turned ON and it activates the energy recovery circuit—thus bypassing the bypass diode. From then on, the energy recovery circuit will start the process of recovering the power from the shaded module, which shall be detailed in the following section. For brevity, in Fig. 1, only two PV modules are shown. However, the system can be expanded to 4, 8, 16, 32 modules, and so on using a simple interconnection scheme.

B. Trigger Circuit

The details of the trigger circuit are shown in Fig. 2. During the normal operation (i.e. uniform irradiance), the proposed circuit is cut-off from the modules. Thus the PV system operates as if the proposed circuit does not exist. However, if partial shading occurs on PV1, for example, its associated bypass diode will be shorted-circuited. The differential amplifier will sense the low voltage (across the diode) and then compare it with a voltage trigger, V_t . If a certain condition is satisfied, the comparator enables the gate signal and thus triggers the energy recovery circuit. Once the recovery circuit is activated, the voltage across PV1 rises. The bypass diode is now open-circuited, and PV1 is directly connected to the energy recovery circuit. Consequently,

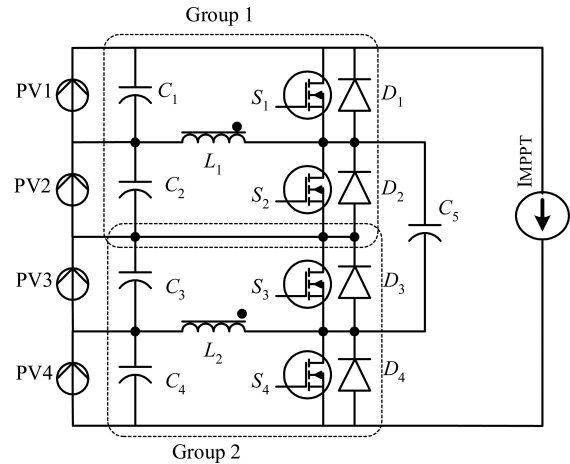


Fig. 3. Basic unit energy recovery circuit.

the process of recovering the power from the shaded module (PV1) begins.

C. Energy Recovery Circuit

Once the partial shading condition is detected, the energy recovery circuit is turned ON by enabling the gate drivers of the switches. To illustrate the recovery concept, a string of four PV modules is used as shown in Fig. 3. For simplicity, a constant current source is used to represent the output power (when multiplied by the PV voltage) drawn from the PV system at MPP. This is acceptable since the objective of the work is to show the effectiveness of the circuit when dealing at the input side of the PV system. This approach is suggested in [41] to avoid complexities in the analysis as well as the simulation. In addition, since the bypass diode is not activated during partial shading, it can be removed to simplify the analysis.

The basic unit of this topology comprises of four PV modules, which is divided into two groups. Group 1 involves PV1 and PV2, together with their corresponding power electronics circuit, comprising of $S_1, D_1, L_1, C_1, S_2, D_2,$ and C_2 . These components form what is referred to (in this paper) as the “within group” circuit. Group 2 includes PV3, PV4 with $S_3, S_4, D_3, D_4, L_2, C_3,$ and C_4 . In order to connect the groups (or “intergroup”), the capacitor C_5 is used. One of the main advantages of the circuit is that the duty cycles of all switches are fixed at 50%. So, only simple control logic is used to control the switches.

Assuming that PV1 is shaded and PV2 receives a full irradiance, PV2 delivers higher current than PV1. However, since the modules are connected in series, the string current will be limited to the amount delivered by PV1. That is why a bypass diode is needed to divert the current away from PV1, or else a hot spot is created in PV1. The main idea behind the proposed method is that, during partial shading, part of the current from PV2 is diverted to the energy recovery circuit (by turning S_2 ON) and the energy is stored temporarily in a storage element, L_1 . By doing so, the string current can be maintained at the level generated by PV1 and hence there is no need for PV1 to be bypassed. As a result, PV1 is still able to actively produce power (albeit in a

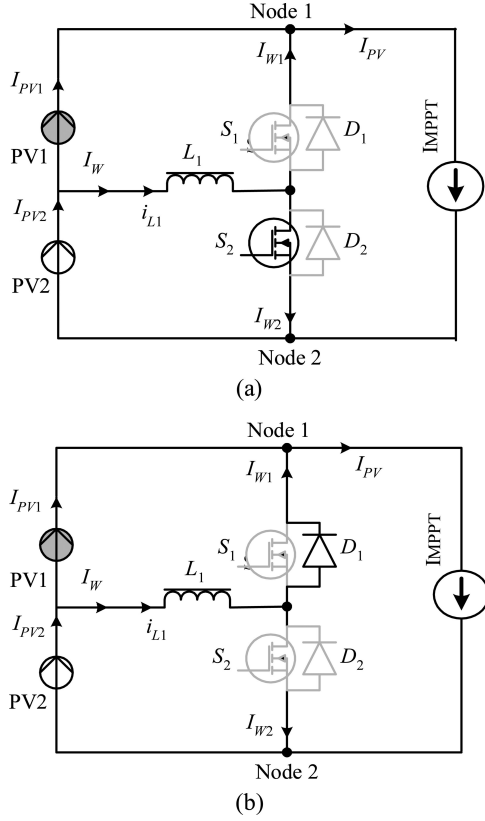


Fig. 4. Circuit operation within group when PV1 is shaded, while PV2 is not shaded: (a) Mode 1 and (b) Mode 2.

lesser amount, depending on the shading condition) because its voltage is not zero. Meanwhile, the energy stored in L_1 will be released back to the output via D_1 (by turning OFF S_2). Thus, ideally, using this scheme, no PV power is wasted except for the losses due to the switches, diodes, and the nonidealities of the passive components. Note that a dead time of 400 ns is applied during transition of the paired switches, for example, between S_1 and S_2 . However, the dead time does not affect the overall behavior of the system.

III. OPERATIONAL MODES AND ANALYSIS

A. Operation “Within-Group”

The operation of the circuit within the group can be divided into two modes, which are defined by the states of the switches in the circuits. During the MPP, both the PV and the load are reacting as a constant current source. Therefore, to simplify the analysis [39], at the MPP, the total current of both PV modules is replaced by a constant current source (I_{MPPT}), as shown in Fig. 4. Furthermore, the nonidealities of the components are also omitted.

Mode 1 ($t_0 < t < t_1$): The operation of the circuit during Mode 1 is shown in Fig. 4(a). Its corresponding timing diagram is shown in Fig. 5. In this mode, S_2 is turned ON, while S_1 is turned OFF. The current flows through S_2 , causing i_{L1} to increase linearly due to the constant voltage supply from PV2. Hence, part of the energy from the nonshaded module (PV2) is

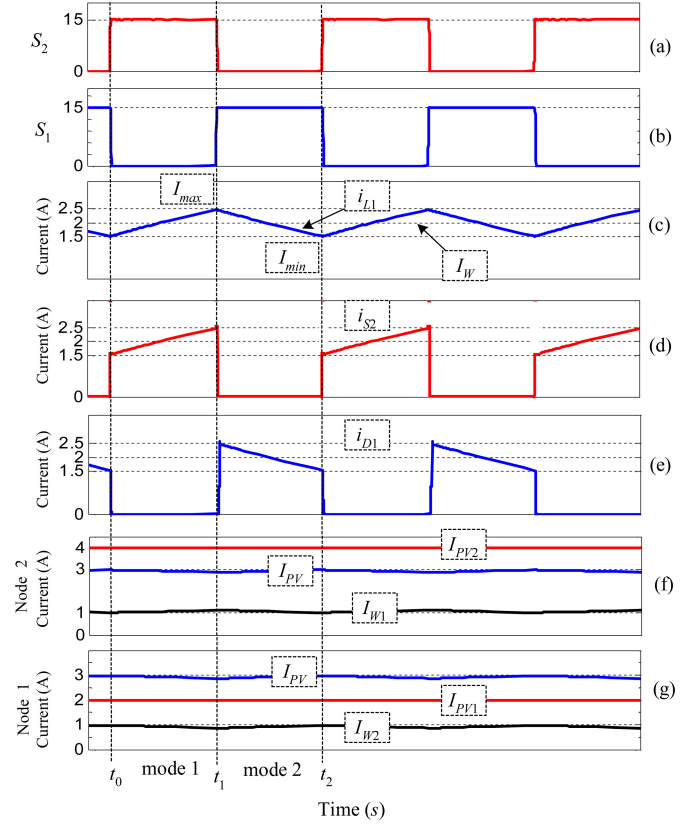


Fig. 5. Timing diagram for group 1 of the proposed method.

temporarily stored in L_1 . This can be understood by observing the current waveforms in trace *c* of Fig. 5. The ripple current of L_1 can be expressed as

$$\Delta I_{L1} = \frac{V_{PV2}DT}{L1} \quad (1)$$

where ΔI_{L1} is the ripple of the inductor current, i.e. ($I_{max} - I_{min}$), while D and T are the duty cycle and the period of the switching, respectively.

Mode 2 ($t_1 > t > t_2$): In this mode, S_1 is turned ON and S_2 is turned OFF, as shown in Fig. 4(b). When S_2 is turned OFF, the current is forced to flow through the freewheeling diode, D_1 . This current is shown by the trace *e* in the timing diagram. The stored energy in L_1 is released in the form of current and flows to the load. Since the duty cycle of the circuit is fixed at 50%, the average inductor current, (i_{L1}) is divided equally to form I_{W1} and I_{W2} . Furthermore, the ac components of I_{W1} and I_{W2} are filtered by the capacitors C_1 and C_2 ; thus, only the dc currents flow to the load. The load current, I_{PV} (which is equal to the average PV string current) at Node 1 can be written as

$$I_{PV} = I_{PV1} + I_{W1} \quad (2)$$

where I_{PV1} is the string current (note: I_{PV1} is limited by the PV1 current). However, at Node 2, the same current can be expressed as

$$I_{PV} = I_{PV2} - I_{W2}. \quad (3)$$

Since the duty cycle is 50%, it follows that

$$I_{W2} = I_{W1} = \frac{I_W}{2}. \quad (4)$$

Therefore

$$\begin{aligned} 2I_{PV} &= I_{PV1} + I_{PV2} \\ I_{PV} &= \frac{I_{PV1} + I_{PV2}}{2}. \end{aligned} \quad (5)$$

Equation (5) indicates that the total current to the load (at MPP) is contributed by the nonshaded module as well as the shaded one. In another word, the proposed circuit acts as a “balancing” element to equalize the currents between the shaded and nonshaded modules such that the current at Node 1 equals Node 2. This implies that during the occurrence of partial shading, the energy from the shaded module is recovered and transferred to the load. Since the output current is increased, while the voltage across the shaded voltage is near its V_{MPP} , the overall energy yield is increased. This is in contrast to the bypass diode method, in which the energy from the shaded module is not usable because the voltage across it is zero.

For further clarification of the concept, the numerical values of currents are used for simulation in Fig. 5. In this case, the PV1 and PV2 currents are 2 A and 4 A, respectively. The resulting average load current is 3 A, which is in accordance with (5).

B. Operation: “Intergroup”

When more than two groups are connected in series (to form a unit), the intergroup connectivity is required. The intergroup operation can be explained using Fig. 6. For clarity, capacitors $C_1, C_2, C_3,$ and C_4 (which act as filters), and L_1 and L_2 are removed because they are not involved in the intergroup interaction. Note that PGV1 is the series combination of PV1 and PV2 after the currents of the shaded and nonshaded modules are successfully balanced. Similarly, PGV2 is a series combination of PV3 and PV4. For the purpose of discussion, PVG1 is designated to be the shaded group, while PVG2 is the nonshaded one.

Mode 1 ($t_0 < t < t_1$): The intergroup operation during *Mode 1* is shown in Fig. 6(a). Its corresponding timing diagram is shown in Fig. 7. In this mode, S_2 and S_4 are simultaneously turned ON, while S_1 and S_3 are turned OFF. The current flows through D_2 and S_4 , causing the capacitor C_5 to be charged. Consequently, part of the energy from the nonshaded group (PVG2) is temporarily stored in C_5 .

Mode 2 ($t_1 > t > t_2$): In this mode, the energy previously stored in C_5 (during *Mode 1*) is released to the output. This is achieved by turning ON S_3 as shown in Fig. 6(b). Since the duty cycle of S_3 is 50%, I_G is divided equally to form I_{G1} and I_{G2} . The MPPT current, I_{PVG} at Node 1 can be written as $I_{PVG} = I_{PVG1} + I_{G1}$. At Node 2, the same current can be expressed as $I_{PVG} = I_{PVG2} - I_{G2}$. Using the similar analysis as in the previous section, the average PV current that flows to the output can be written as

$$I_{PVG} = \frac{I_{PVG1} + I_{PVG2}}{2}. \quad (6)$$

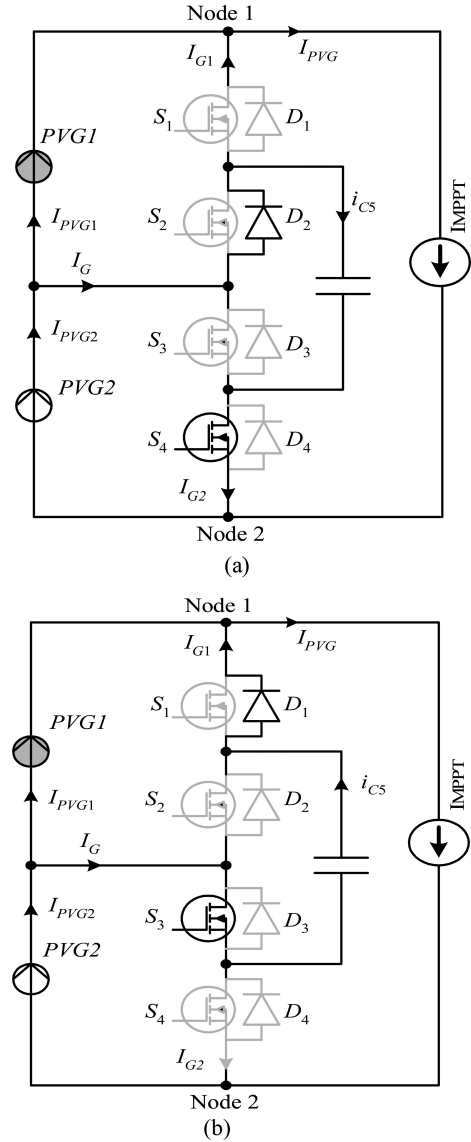


Fig. 6. Circuit operation intergroup when group 1 is shaded, while group 2 is not shaded: (a) Mode 1 and (b) Mode 2.

From (6), it can be observed that the total MPPT current is the contribution by the nonshaded intergroup as well as the shaded one. Effectively, the circuit provides a path for higher current of the nonshaded group to flow so that the current from the shaded group can be utilized. It should be noted that if a bypass diode is used, the voltage across the shaded modules is zero; consequently, no power can be harvested from them.

The proposed circuit that comprises of eight modules (two units) is shown in Fig. 8. It requires additional two switches (S_9 and S_{10}) and an inductor (L_5) to nestle the two units together. The operation of this circuit is similar to the intergroup situation. However, in this case, PV1 through PV4 are considered as one unit, while PV5 through PV8 is another unit. Using the same intergroup concept, the connectivity can be established by manipulating S_9 and S_{10} in conjunction with L_5 . Note that, by this manner the number of modules can be expanded to 16, 32, 64, and so on.

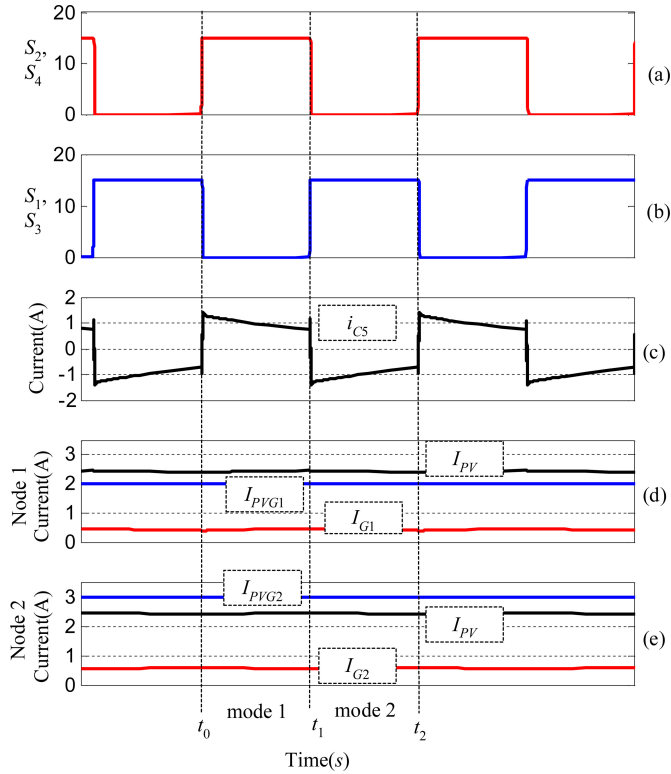


Fig. 7. Timing diagram of intergroup operation of the proposed method.

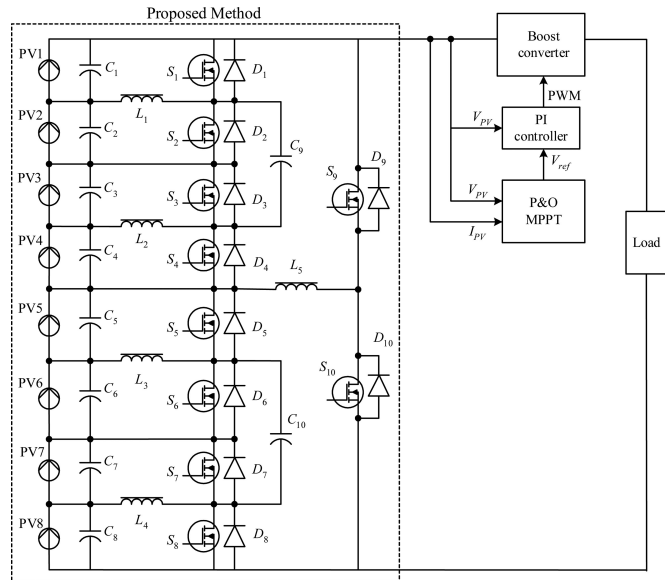


Fig. 8. Proposed circuit with eight PV modules.

Table I(b) summarizes the states of all switches and diodes, as well as the charging and discharging of inductor and capacitors for eight modules. Different partial shading conditions are imposed, as shown in Table I(a). To be consistent with the earlier analysis, the modules are intergrouped and labeled as follows: [PVG1 = PV1 + PV2], [PVG2 = PV3 + PV4], [PVG2 = PV5 + PV6], and [PVG4 = PV7 + PV8]. In addition, the nested intergroup is defined as: [PVBG1 = PVG1 + PVG2] and [PVBG2 = PVG3 + PVG4]. At the output side of the circuit,

TABLE I
(a) SHADING CONDITIONS FOR EIGHT MODULES. (b) STATES OF SWITCHES, INDUCTORS, AND CAPACITORS WHEN SUBJECTED TO SHADING CONDITIONS GIVEN IN TABLE I(a)

(a)

| | Condition | 1 | 2 | 3 | 4 |
|---------------------------|-----------|-----|-----|-----|-----|
| PV Irradiation in Sun (S) | PV1 | 0.5 | 1.0 | 1.0 | 1.0 |
| | PV2 | 1.0 | 0.5 | 1.0 | 1.0 |
| | PV3 | 1.0 | 1.0 | 1.0 | 0.5 |
| | PV4 | 1.0 | 1.0 | 1.0 | 1.0 |
| | PV5 | 1.0 | 1.0 | 0.5 | 0.5 |
| | PV6 | 1.0 | 1.0 | 1.0 | 1.0 |
| | PV7 | 1.0 | 1.0 | 1.0 | 1.0 |
| | PV8 | 1.0 | 1.0 | 1.0 | 1.0 |

(b)

| | Condition | 1 | 2 | 3 | 4 |
|--------|------------------------------|---------------|----------|----------|------------|
| Mode 1 | Switch that conducts current | S_2, S_{10} | S_{10} | S_6 | S_4, S_6 |
| | Diode that conducts current | | D_2 | D_{10} | |
| | Inductor being charged | L_1, L_5 | L_5 | L_3 | L_2, L_3 |
| | Inductor being discharged | | L_1 | L_5 | |
| | Capacitor being charged | C_9 | C_9 | C_{10} | C_{10} |
| | Capacitor being discharged | | | | C_9 |
| Mode 2 | Switch that conducts current | | S_1 | S_9 | |
| | Diode that conducts currents | D_1, D_9 | D_9 | D_5 | D_3, D_5 |
| | Inductor being charged | | L_1 | L_5 | |
| | Inductor being discharged | L_1, L_5 | L_5 | L_3 | L_2, L_3 |
| | Capacitor being charged | | | | C_9 |
| | Capacitor being discharged | C_9 | C_9 | C_{10} | C_{10} |

the boost converter (with P&O MPPT), the PI controller, and the load are interconnected to emulate the I_{MPPT} (as shown in Fig. 6).

As an example, for shading Condition 1, only PV1 is shaded. It receives 0.5 S ($1.0 \text{ S} = 1.0 \text{ kW/m}^2$) while the rest of the modules are fully irradiated (at 1.0 S). During *Mode 1*, S_2 conducts the current and starts to charge L_1 . In *Mode 2*, D_1 is conducting, and the energy is discharged from L_1 . In order to allow for higher current from PVG2 to flow to the output, it needs a new current path, which is provided by C_9 . In this situation, C_9 allows the energy to be transferred from PVG2 to PVG1 by storing it during *Mode 1*, and releasing it during *Mode 2*. Furthermore, it can be observed that the total irradiation of (nested intergroup) PVBG1 is less than PVBG2. Due to the unbalanced irradiation, another current path is required to allow the energy from PVBG2 to flow to the output. This path is provided by L_5 ; it is charged through S_{10} during *Mode 1* and discharged through

D_9 in *Mode 2*. The operation for Conditions 2 and 3 are similar as above, but the modules are subjected to different shading patterns. For Condition 4, the total of irradiation of PVBG1 and PVBG2 is equal, but the shading locations are interchanged. There is no need to provide a current path between PVBG1 and PVBG2; both S_9 and S_{10} can be turned OFF. However in this work, S_9 and S_{10} are turned ON and OFF alternately, in synchronization with S_1 and S_2 .

IV. EXPERIMENTAL SETUP

A. Simulation Model

The proposed energy recovery system is validated using MATLAB-Simulink simulation as well as experimental prototype. Two sets of experiments are carried out. The first set utilizes four PV modules, i.e. one unit. The purpose is to verify the analysis given in Section III. The second experiment is using eight (two units) modules, as shown in Fig. 8. For the PV simulation, the two-diode model of the solar cell is used [42] as it gives more accurate results than the more popular single diode model. For consistency, the same circuit is used for hardware verification. Experimentally, the BP-MSX60 PV module is used. Its peak rated power is 60 W (3.5 A/17.1 V) at standard test conditions (STC). The original manufactured module is modified (by rearranging its internal wiring) such that it becomes two modules (8.55 V, 30 W each). Thus the totally rated power for the experimental rig at STC is 240 W.

B. Power Circuit

The power circuit is constructed using ten IRFB4332 PBF MOSFETs. This device has an integrated freewheeling diode; thus no (additional) external diode is required. The values of inductors ($L_1 - L_4$) are 500 μ H. These are computed by considering the allowable inductor current ripple, based on (1). The capacitors ($C_1 - C_4$) are chosen to be 100 μ F; the values are derived by simulation. The PV (along with the proposed circuit) is connected to a boost converter. The latter is equipped with the P&O MPPT algorithm. The boost converter has the following specifications: switching frequency, $f = 40$ kHz, filter capacitor, $C = 500$ μ F, and boost inductor, $L = 500$ μ H. A 70- Ω resistor is used to represent the load. Similarly, the boost converter uses the IRFB4332PBF and BYW29EX-200 for its switch and diode, respectively. To measure the PV voltage, V_{PV} , a simple voltage divider is used. Furthermore, an LEM brand current transducer, rated at 10 A is selected for the I_{PV} current measurement. In addition, a low cost 16-bit Infineon XC167 microcontroller is used to implement the MPPT algorithm. A PI controller is applied to maintain the PV voltage, V_{PV} , at the voltage reference, V_{ref} . The PI controller is manually tuned such that the steady state condition is reached in less than 20 ms.

C. Solar Simulator

In other work [6], [41], it is assumed that during partial shading, the shaded modules are considered to be 100% shaded. This assumption, in practice, might not be accurate because, typically, the shaded module still receives a certain amount of

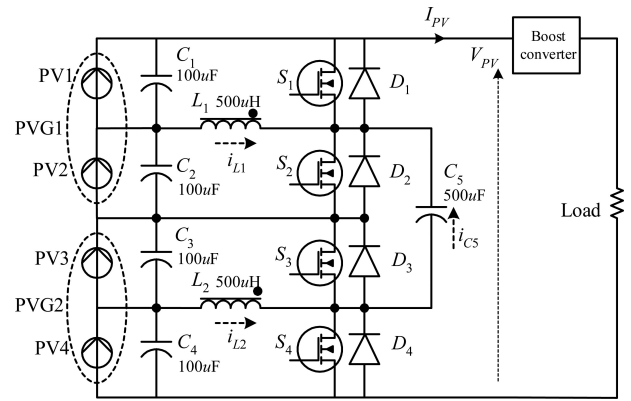


Fig. 9 Circuit used to validate the concept of the proposed energy recovery circuit.

energy. Thus, it is not sufficient just to partially shade the modules and assume it receives zero irradiance. Rather, the amount of shading must be known so that performance of the proposed circuit can be quantified. To create a controllable irradiance condition, an in-house solar simulator is designed and built. It is constructed using an array of tungsten-halogen light bulbs, each rated at 50 W. Although the application of tungsten-halogen is not ideal [43], it has been used in other similar works, for example in [44]. The BP-MSX60 PV module (which is split into two, with dimension of 47 in \times 10 in each) is illuminated by 18 unit of these bulbs. To avoid disturbance by a 100-Hz ripple (from ac source), the bulbs are powered by dc sources. The irradiance is varied by controlling the intensity of the bulbs using the dc light dimmer circuit. At all times, the irradiance and temperature are measured using an irradiance meter and a temperature sensor, respectively. The simulation conditions (especially the parameters of the two-diode model) are adjusted to match the measured irradiance and temperature when the actual readings are taken.

V. RESULTS AND DISCUSSIONS

A. Validation of the Energy Recovery Concept

To validate the concept and analysis of the proposed energy recovery circuit, experiment using four modules (configured as one unit) is carried out. The case is made similar to the one described in Section III. For ease of referencing, the circuit is redrawn again as in Fig. 9. To ensure consistency, both validation methods, i.e. simulation and hardware, use the same component values and parameters. The irradiance conditions for the modules are designated as follows: PV1 = 0.3 S, PV2 = 0.3 S, PV3 = 0.5 S, and PV4 = 0.6 S.

Fig. 10 shows the key waveforms of the simulated circuit, while the hardware results are represented by the oscillograms shown in Fig. 11. Note that Fig. 11 has to be divided into subparts (a) and (b) because the oscilloscope can only display four channels at a time. Since the irradiances for PV1 and PV2 are the same, the power generated by both modules is balanced. Therefore, during *Mode 1*, i.e. S_1 and S_3 are turned OFF (and S_2, S_4 are turned ON), the current (i_{L1}) that flows into its corresponding storage inductor (L_1) has an average value of

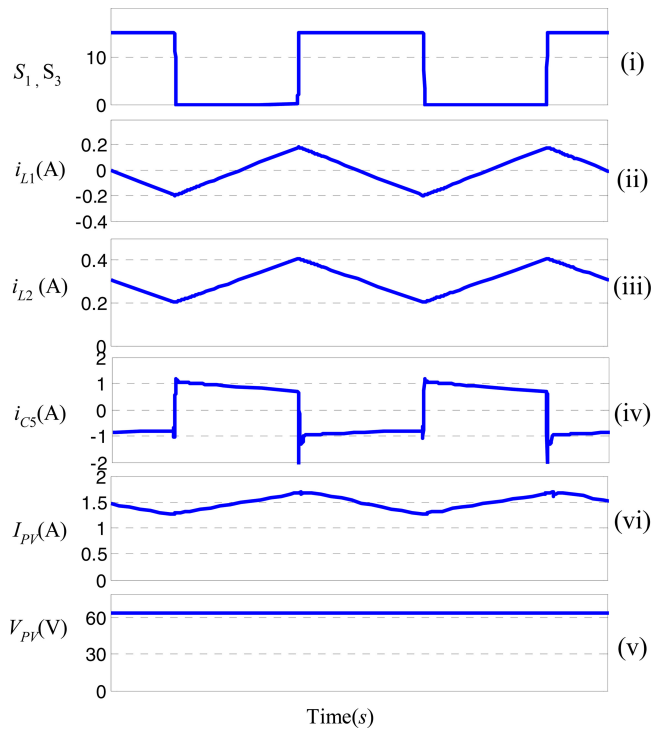


Fig. 10 Simulated timing diagram of circuit in Fig. 9. Trace (i): switching signal S_1, S_3 , trace (ii): inductor current, i_{L1} , trace (iii): inductor current, i_{L2} , trace (iv): capacitor current, i_{C5} , trace (v): PV output current, I_{PV} , and trace (vi): PV output voltage, V_{PV} .

zero. This fact can be observed in the simulation (trace (ii) of Fig. 10) and verified by the hardware results of Fig. 11(a). To relate it with the analysis in Section III, these two modules are grouped as PVG1. On the other hand, PV3 and PV4 (group PVG2) receive different amount of irradiances; thus each module generates different amounts of power. The energy imbalance causes a current (i_{L2}) with an average value of approximately 280 mA to flow into L_2 . This is depicted by trace (iii) in Fig. 10 and similar result is obtained from the practical circuit. Furthermore, since the energy received by PVG1 is less than PVG2, the capacitor C_5 is charged through i_{C5} . This takes place during *Mode 1*. During this interval, the energy is temporarily stored in C_5 . Finally, when S_1 and S_3 are turned ON (*Mode 2*), the energy is released to the output by discharging C_5 , via I_{PV} . This phenomena can be observed by trace (iv) of Fig. 10. The results from simulation are closely followed by the practical waveforms in Fig. 11(a).

B. Dynamic Response

To show the effectiveness of the proposed circuit in recovering the power from the shaded modules, the PV system is switched from the bypass diode (mode) to the proposed circuit (mode). The eight modules are subjected to the following shading patterns: PV1 = 0.25 S, PV 2 = 0.25 S, PV3 = 0.5 S, PV4 = 0.7 S, PV 5 = 1.0 S, PV6 = 1.0 S, PV7 = 1.0 S, and PV8 = 1.0 S. The corresponding P - V curves for the bypass diode and the proposed method are simulated and are shown as trace 1 (blue) and trace 2 (red), respectively, in Fig. 12(a). As expected, using

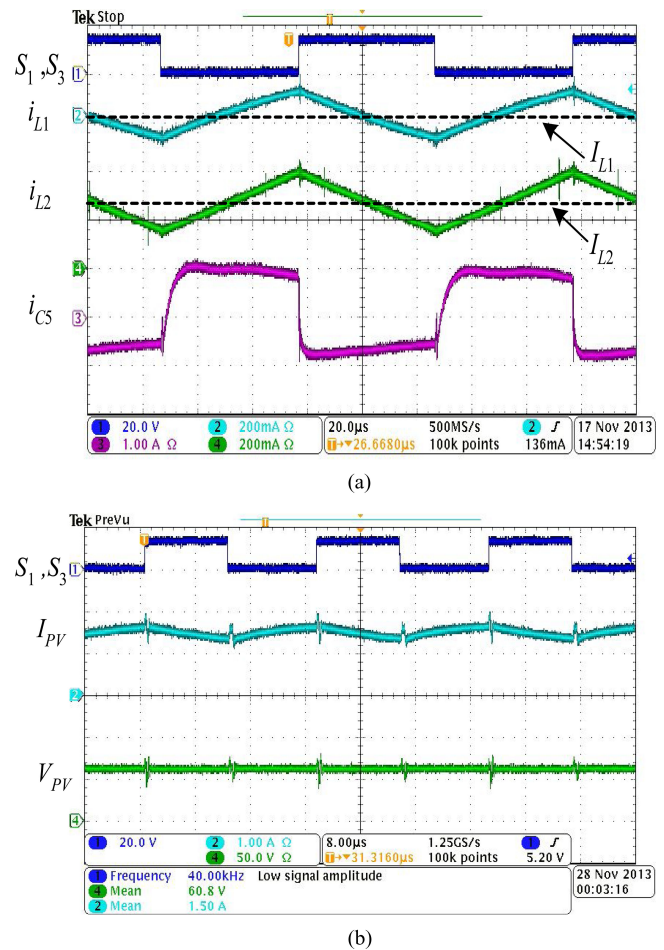


Fig. 11 (a) Oscilloscope from hardware of circuit in Fig. 9. Switching signal, S_1, S_3 (20 V/div), inductor current, i_{L1} (200 mA/div), inductor current, i_{L2} (200 mA/div), capacitor current, i_{C5} (1 A/div). (b) Oscilloscope from hardware of circuit in Fig. 9. Switching signal, S_1, S_3 (20 V/div), PV output current, I_{PV} (1 A/div), and PV output voltage, V_{PV} (20 V/div).

the bypass diode, a multiple peak P - V curve is obtained. On the other hand, for the proposed circuit, the curve exhibits only a single peak because effectively, the modules are “balanced,” i.e. as if the partial shadings have not occurred. Also, note that this peak is much higher than the global peak of the P - V curve with the bypass diode.

For the system with the bypass diode, it is assumed that the P&O algorithm successfully locates the global peak at (43 V, 93 W). This point is designated as GP1 in Fig. 12(a). It has to be noted that such condition is the best possible scenario and may not necessarily be true as the MPPT algorithm may be trapped at one of the local peaks. In such a case, the output power could be much lesser. Experimentally, this point is verified by the power trace (red) in the oscilloscope of Fig. 12(b). However, in the practical case, the achieved voltage and power is a bit lower, i.e. 40 V and 90.5 W, respectively. The difference between the simulated and experimental result is acceptable, considering 1) the voltage drop across the bypass diode and 2) the power losses due to the activation of the diode. Another possible cause for the minor discrepancies is the variation in the temperature of the modules that has risen during the experiment.

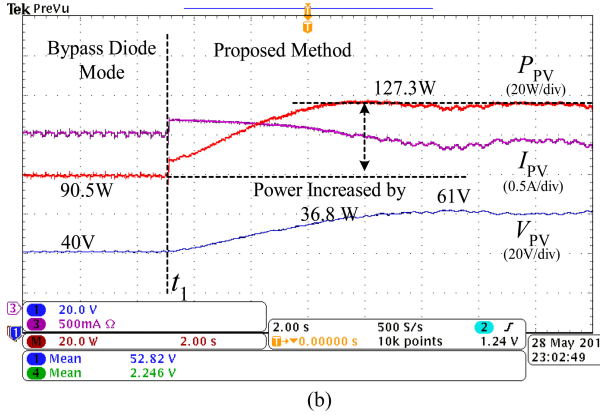
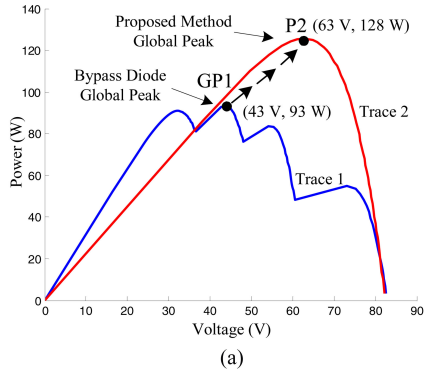


Fig. 12. MPPT response when the PV system is switched from the bypass diode mode to the proposed method. (a) Simulated P - V curve. (b) Experimental results.

TABLE II

CONDITIONS FOR THE STEP CHANGE IN IRRADIANCE IN SUN (S). NOTE: UNIT SUN EQUALS 1000 W/m^2 AT STC

| Condition | PV1 | PV2 | PV3 | PV4 | PV5 | PV6 | PV7 | PV8 |
|-----------|------|------|------|------|------|------|------|------|
| 1 | 0.25 | 0.24 | 0.50 | 0.68 | 0.97 | 0.97 | 0.97 | 0.95 |
| 2 | 0.25 | 0.24 | 0.50 | 0.68 | 0.48 | 0.55 | 0.49 | 0.48 |

At t_1 , the system is switched to the proposed circuit mode. From the simulation in Fig. 12(a), the peak moves to a new global point (63 V, 128 W) as pointed by P2 in the P - V curve. Experimentally, this movement can be observed in the oscillogram shown in Fig. 12(b). The P&O begins its tracking toward the new MPP (following the direction of the arrow) and finally settles at (61 V, 127.3 W). Thus, from this experiment, it can be concluded that by applying the proposed scheme, the output power is increased significantly, in this particular shading case by 36.8 W (29%). The slow tracking time is due to the small voltage step size of the P&O; if the step size is chosen to be larger, the tracking speed would be faster. However, this is achieved at the cost of larger steady state oscillation.

C. Rapid Change in Shading Patterns

Fig. 13 illustrates the response of the PV system with the bypass diode when the irradiance pattern is changed very quickly. The shading patterns are depicted in Table II. Initially, the shading patterns for the eight modules are subjected to Condition 1 of Table II. The corresponding P - V curve for this pattern is shown

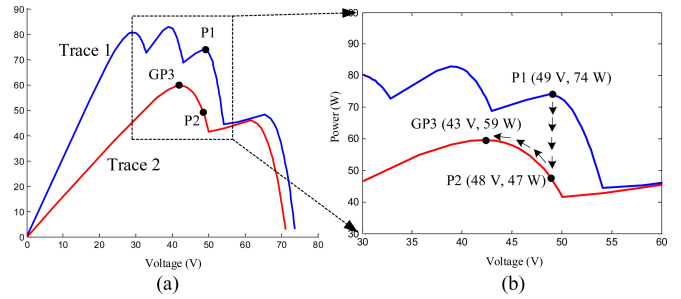


Fig. 13. (a) P - V curve in bypass diode mode, with the shading condition shown in Table II. (b) Enlargement of (a).

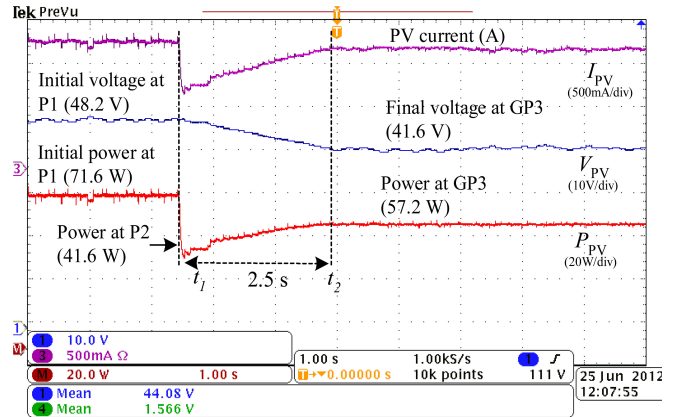


Fig. 14. Dynamic response of the bypass diode mode with the shading condition based on curves in Fig. 13.

in trace 1 of Fig. 13(a); for this case, the curve has four peaks. It is assumed that the PV is initially operated at a maximum point, P1 (48.2 V, 71.6 W). Note that, P1 is not the true global peak due to the fact that the P&O is already trapped at a local peak. When the irradiance is changed to Condition 2, the PV system is now characterized by trace 2. Under this condition, the curve consists of two peaks. For clarity, the enlargement of the PV curves is shown as an inset of Fig. 13(b). As can be observed, the change in the shading pattern forces the operating point to move from trace 1 to trace 2, i.e. the power drops from P1 and hits P2 (48.2 V, 41.6 W). From this point, the P&O algorithm starts the climbing process (to search for the peak) and finally settles at a new peak, GP3 (41.6 V, 57.2 W).

The movements of the PV operating points are verified experimentally. The oscillogram in Fig. 14 clearly marks all the critical points observed during the changes. By applying Condition 1 in Table II, the initial voltage and the power are found at 48.2 V and 71.6 W, respectively. These values correspond correctly to P1 in the P - V curves described in Fig. 10(a). At t_1 , the shading is changed to Condition 2 (in one step, using a control switch); consequently, the operating power drops from 71.6 to 41.6 W. The voltage, however, remains constant at 48.2 V. Again, these values agree very closely with simulation. From here, the power starts to climb as the P&O algorithm begins its search for the new global peak. Meanwhile, the voltage drops accordingly, following trace 2. It finally reaches GP3 and settles to this final value in 2.5 s. Since the sampling period for

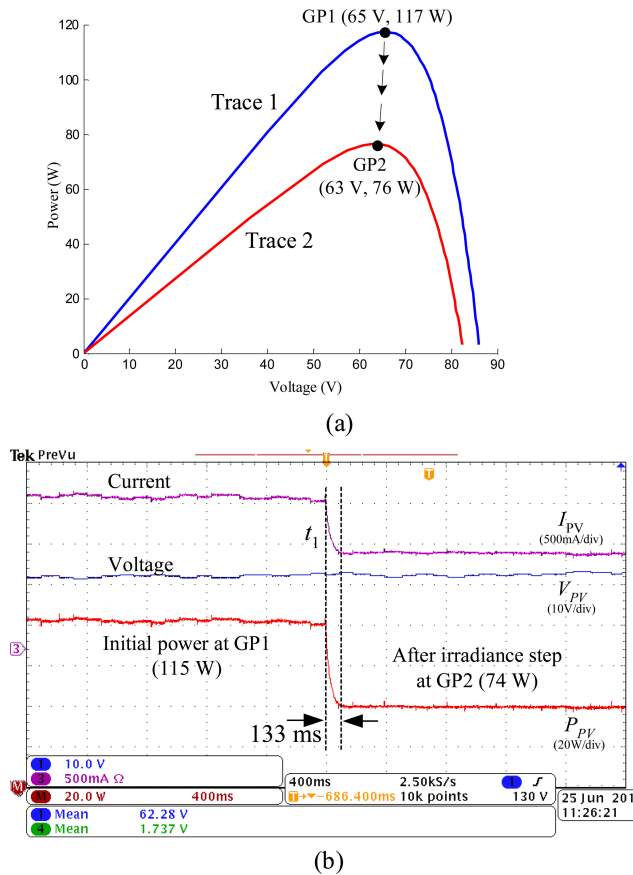


Fig. 15 (a) P - V curve for the proposed method with the shading condition shown by Table II. (b) Dynamic response of the proposed method for the curves in (a).

the MPPT controller is 100 ms, the P&O requires 25 cycles to complete the search for the new peak, i.e. from P1 to GP3.

Fig. 15 demonstrates the performance of the proposed method for a step change in irradiance, for the same conditions given in Table II. The corresponding P - V curve is shown in traces 1 and 2 of Fig. 15(a), respectively. Again, note that for the proposed method, the curve consists only of a single peak, which is advantageous with regards to MPPT implementation. Initially, due to Condition 1, the simulation maximum point is located at GP1 (65 V, 117 W). This point is also correctly shown in the oscillogram of Fig. 15(b), i.e. the oscillation is on average at (62 V, 115 W). When the shading condition is changed to Condition 2, the PV characteristic changes from trace 1 to trace 2; accordingly, the operating point moves from GP1 to GP2. The latter point is 63 V, 76 W. Experimentally, the step change in irradiance is introduced at time t_1 . As can be seen from the oscillogram in Fig. 15(a), the power drops to 74 W, while the voltage is maintained at approximately 62 V. Furthermore, since the proposed system does not have multiple peaks, GP2 is located directly below GP1 in the P - V curve. Consequently, even with a large step change in irradiance, the difference in the operating voltage between the two global peaks is very small. As a result, the P&O is able to track GP2 very quickly, i.e. within one to two MPPT control cycles, or 133 ms, as indicated in Fig. 15(b).

TABLE III
SHADING PATTERNS. NOTE: CONDITION 6 IS FOR BENCHMARKING PURPOSE, i.e., NO PARTIAL SHADING IS IMPOSED

| Module | Irradiation for shading conditions (S) | | | | | |
|--------|--|------|------|------|------|------|
| | 1 | 2 | 3 | 4 | 5 | 6 |
| PV1 | 1.00 | 1.00 | 0.25 | 0.70 | 0.25 | 1.00 |
| PV2 | 1.00 | 1.00 | 0.25 | 1.00 | 0.25 | 1.00 |
| PV3 | 1.00 | 1.00 | 0.50 | 1.00 | 0.25 | 1.00 |
| PV4 | 0.70 | 0.25 | 0.70 | 1.00 | 1.00 | 1.00 |
| PV5 | 1.00 | 0.25 | 1.00 | 0.70 | 1.00 | 1.00 |
| PV6 | 1.00 | 1.00 | 1.00 | 0.50 | 0.50 | 1.00 |
| PV7 | 1.00 | 1.00 | 1.00 | 0.50 | 0.50 | 1.00 |
| PV8 | 1.00 | 1.00 | 1.00 | 1.00 | 1.00 | 1.00 |

From these observations, another important feature of the proposed method can be deduced: for the standard P&O, there is always a possibility that the algorithm will be trapped at the local peak. The inability to differentiate between the local and global peaks is a well-known drawback of the P&O algorithm [13], [17]. As such, more complicated MPPT algorithms (that can cater for partial shading), for example [6], [13], need to be considered. On the other hand, with the proposed technique, the global peak will always be tracked by a standard P&O because the multiple peaks simply do not exist. Being trapped at a local peak is not an issue.

D. Efficiency

To investigate the efficiency improvement of the proposed method, five irradiance patterns, representing various possible partial shading scenarios are simulated using a string of eight modules. These patterns are arbitrarily selected and are shown in Table III; they are labeled as Conditions 1 through 5. The efficiencies are benchmarked to the efficiency during the absence of partial shading, i.e. Condition 6. For simplicity, four irradiation values, i.e. 1.0, 0.7, 0.5, and 0.25 S are used to represent different levels of shading intensities ($1.0 \text{ S} = 1.0 \text{ kW/m}^2$). Again, the BP-MSX60 PV module is used. Each module is derated to 25 W at 35°C , giving the total power (ideal) of 200 W for the eight modules. For the validation, the experiment using the same simulation scenario is carried out. Furthermore, when the system is in the bypass diode mode, a semimanual control is applied for the MPPT algorithm to ensure that the operating point always matches the global peak. (Note: The P&O MPPT cannot consistently track the global peak under partial shading condition.)

The simulation and the experimental results are shown in Table III. For clarity, they are summarized as bar charts in Fig. 17. The first row (P_{SUM}) indicates the maximum achievable power that can be generated by the eight modules if the contribution from each module is summed individually. P_{SUM} also implies the true location of MPP for each module under various shading conditions. Thus, by definition, the efficiency

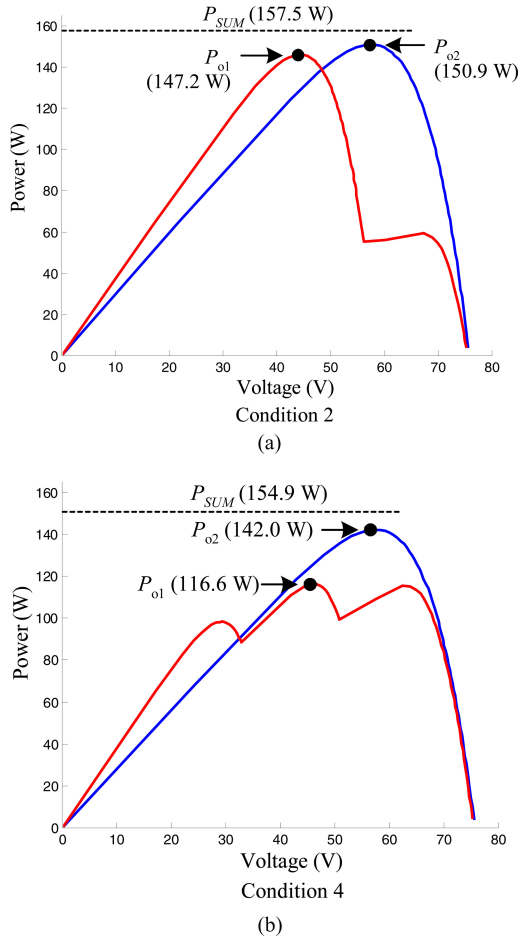


Fig. 16. P - V curves generated by the proposed method and the bypass diode method (a) under Condition 2 and (b) under Condition 4 of Table III. (Note: P_{o1} is the maximum power achievable from the eight string for the bypass diode; P_{o2} is the maximum power achievable from the eight string for the proposed method.)

of the proposed system is computed as follows [45]:

$$\eta = \frac{P_o}{P_{SUM}} \quad (7)$$

where P_o is the maximum output power delivered by the string, i.e. $I_{PV} \times V_{PV}$ minus the converter losses, when the modules are subjected to the shading pattern.

For the nonshading condition (Condition 6, i.e. the benchmark), the simulated P_{SUM} is 197.2 W. Since the P&O operates ideally, $P_o = P_{SUM}$. Consequently, the efficiency is 100%. Furthermore, because all modules are uniformly irradiated, neither the bypass diode nor the proposed circuit is activated. For other conditions (1 through 5), the efficiency varies according to the shading pattern imposed on the modules. For example, for Condition 2, the simulated efficiencies of the bypass diode and the proposed method are quite high (94 and 95%, respectively). This is because their P_o is close to P_{SUM} . Alternatively, this fact can be confirmed by plotting their corresponding P - V curves, as shown in Fig. 16(a). As can be seen, the peak power for bypass diode (P_{o1}) is 147.2 W, while for the proposed method, the peak power (P_{o2}) is 150.9 W. In another scenario, the shading pattern

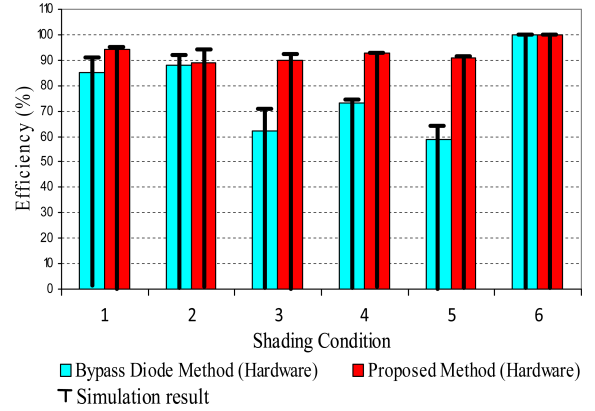


Fig. 17. Comparison of the system efficiency [as defined by (7)] of the bypass diode and the proposed method (simulation and experimental) for selected partial shading conditions.

imposed by Condition 4 results in a significant loss of power for the bypass diode (38.3 W). This causes its efficiency to drop to 75.3%. For the proposed method, the power loss is much lower (12.9 W); hence, its efficiency remains high, i.e. 93%. These facts can be related to the corresponding P - V curve, as shown in Fig. 16(b). Generally, the efficiency of the proposed method is relatively high, (i.e. above 90%), even in the case of severe shading, for example in Condition 5. The last row of Table IV computes the additional power that can be harvested (using the proposed method) to be part of the output power. This is the amount of power that is recovered from the shaded modules, which otherwise will be wasted if the bypass diodes are activated. However, a generalized formula for the recovered power could not be easily quantified due to its dependence on a specific shading pattern. However, from Table IV, in general, there is a consistent trend between the simulated and the experimental efficiencies. The agreement between the two can be further observed by the bar graphs in Fig. 17. From these correlations, two conclusions can be suggested: 1) the concept of energy recovery using the proposed method is verified and 2) the experimental rig (built using the tungsten-halogen bulbs) is adequate for the purpose of this study.

Another important point to note is that, for the bypass diode, it is assumed that the P&O successfully locates the global peak. In a real situation, this may not be necessarily the case. If the P&O is trapped at one of the local peaks, P_o might become much lower and so does the efficiency. Hence, the computed efficiency shown in Table IV is actually the best possible case achievable for the bypass diode. On the contrary, for the proposed method, P_o is always unique because it has only one global peak.

There is another explanation why the total power that can be extracted by the proposed method could not reach the theoretical value of P_{SUM} under partial shading: the low MPPT efficiency, η_{MPPT} . Recall that the duty cycles of the switches are fixed at 50%. Since the circuit is opened-loop, under different irradiance, the voltage of every module could not be regulated to V_{MPP} . To demonstrate this fact, a simulation is conducted using eight modules with shading conditions as shown in Table V. The P - V curve for every individual module is plotted in Fig. 18. As can

TABLE IV
SIMULATED AND EXPERIMENTAL RESULTS FOR SHADING PATTERNS IMPOSED ON THE BYPASS DIODE AND THE PROPOSED CIRCUIT
(SIM: SIMULATION; EXP: EXPERIMENTAL)

| | | Condition | | | | | | | | | | | |
|--|--------------|-----------|-------|-------|-------|-------|-------|-------|-------|-------|------|------------------|-------|
| | | 1 | | 2 | | 3 | | 4 | | 5 | | 6 (Benchmark) | |
| | | Sim | Exp. | Sim | Exp. | Sim | Exp. | Sim | Exp. | Sim | Exp. | Sim | Exp. |
| $P_{SUM}(W)$ | | 188.8 | 179.3 | 157.5 | 141.9 | 136.7 | 135.0 | 154.9 | 157.5 | 112.0 | 98.9 | 197.2 | 182.7 |
| $P_o(W)$ | Bypass diode | 171.9 | 152.0 | 147.4 | 125.5 | 101.1 | 84.2 | 116.6 | 115.0 | 73.8 | 58.6 | 197.2 | 182.7 |
| | Proposed | 181.8 | 168.0 | 150.9 | 127.0 | 128.2 | 122.0 | 142.0 | 146.0 | 102.7 | 90.1 | 197.2 | 182.7 |
| System Efficiency (%) $\frac{P_o}{P_{sum}}$ | Bypass diode | 91.0 | 84.7 | 93.6 | 88.0 | 73.9 | 62.3 | 75.3 | 73.0 | 65.9 | 59.2 | 100.0 | 100 |
| | Proposed | 96.3 | 93.6 | 95.8 | 89.4 | 93.8 | 90.3 | 93.0 | 92.6 | 91.7 | 91.0 | 100.0 | 100 |
| Recovered Power (using the proposed method) | in (W) | 9.9 | 16.0 | 3.5 | 1.5 | 27.1 | 37.8 | 25.4 | 31.0 | 28.9 | 31.5 | 0.0 | 0.0 |
| | in (%) | 5.2 | 8.9 | 2.2 | 1.1 | 19.8 | 28.0 | 16.4 | 19.6 | 25.8 | 31.8 | 0.0 | 0.0 |

TABLE V
CONDITIONS TO TEST THE DIFFERENCE BETWEEN THE TRUE AND THE OPERATING MPP

| Module | Irradiance (S) | True MPP voltage (V) | Operating MPP voltage (V) | True MPP power (W) | Operating MPP Power (W) |
|-----------------------|----------------|----------------------|---------------------------|--------------------|-------------------------|
| PV1 | 1.00 | 17.30 | 17.80 | 59.91 | 59.50 |
| PV2 | 0.90 | 17.20 | 15.38 | 52.77 | 50.82 |
| PV3 | 0.80 | 17.00 | 17.80 | 50.27 | 46.25 |
| PV4 | 0.95 | 17.20 | 15.30 | 56.69 | 53.71 |
| PV5 | 0.85 | 17.10 | 17.80 | 53.47 | 52.88 |
| PV6 | 0.70 | 16.80 | 15.30 | 40.73 | 39.25 |
| PV7 | 0.60 | 16.50 | 17.70 | 34.45 | 33.25 |
| PV8 | 0.50 | 16.30 | 15.40 | 28.25 | 27.78 |
| Total power generated | | | | 376.54 | 363.44 |

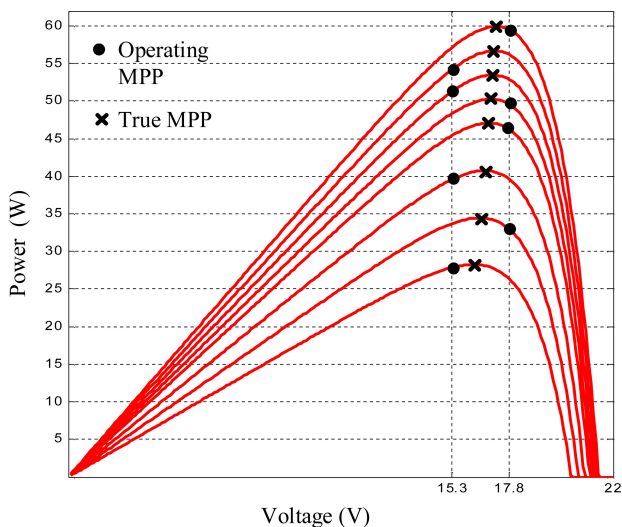


Fig. 18. Operating point of each individual PV module for irradiance conditions given in Table V.

be seen, the operating point (i.e. the voltage of the PV) does not necessary match the true MPP. For example, for PV2, the true MPP is 17.2 V, while the operating point is only 15.38 V. Consequently, the power is reduced from 52.77 to 50.86 W. Similar reductions can be seen for other shading conditions. In overall, the reduction is reflected by the MPPT efficiency, η_{MPPT} . In this case, η_{MPPT} is 96.5%.

From this illustrative example, it is acknowledged that for most shading conditions, the proposed circuit will yield $\eta_{MPPT} < 100$. This is to be expected because a fixed duty cycle is employed for each switch. To ensure every module operates at its unique MPP, a closed-loop MPPT for every module must be employed, for example as proposed in [12]. However, to control every switch is costly because it needs additional microcontrollers, sensors, and separate dc power supplies. As the number of modules gets larger, the complexity of the energy recovery circuit grows considerably; consequently, the system may no longer be practical. In addition, the individual switch needs to be synchronized with the MPP controller of the central inverter, thus losing its (flexible) retrofitting feature. Based on these considerations, it is more feasible for the proposed circuit to remain opened-loop. Despite this drawback, in most cases, the proposed circuit is very effective and is able to recover substantial amount of energy during partial shading, as proven by the results shown in Table IV.

VI. CONCLUSION

A simple circuit is proposed to increase the output power of the PV system during partial shading. The idea is to take the current from the nonshaded module, divert it using a power electronics circuit, and process it to become part of the output power. Consequently, the inclusion of the proposed circuit enables the system to deliver more power compared to the conventional bypass diode method. Simulation results show marked

improvement in the output power, especially under heavy partial shading condition. Experimental work has shown excellent agreement with the simulation. Experimental results show that using the scheme, the efficiency of the system can be increased up to 32%, compared to the bypass diode method. The improvement is more significant for the case of severe shadings. The extra power generated is expected to compensate for the cost of the extra components in the retrofit circuit and generates profit in the long run.

REFERENCES

- [1] A. Maki and S. Valkealahti, "Power losses in long string and parallel-connected short strings of series-connected silicon-based photovoltaic modules due to partial shading conditions," *IEEE Trans. Energy Convers.*, vol. 27, no. 1, pp. 173–183, Mar. 2012.
- [2] J. M. A. Myrzik and M. Calais, "String and module integrated inverters for single-phase grid connected photovoltaic systems—a review," in *Proc. 2003 IEEE Bologna Power Tech. Conf.*, 2003, vol. 2, pp. 430–437.
- [3] H. Haibing, S. Harb, N. Kutkut, I. Batarseh, and Z. J. Shen, "A review of power decoupling techniques for microinverters with three different decoupling capacitor locations in PV systems," *IEEE Trans. Power Electron.*, vol. 28, no. 6, pp. 2711–2726, Jun. 2013.
- [4] E. Koutroulis and F. Blaabjerg, "Design optimization of transformerless grid-connected PV inverters including reliability," *IEEE Trans. Power Electron.*, vol. 28, no. 1, pp. 325–335, Jan. 2013.
- [5] L. Yanlin and R. Oruganti, "A low cost flyback CCM inverter for AC module application," *IEEE Trans. Power Electron.*, vol. 27, no. 3, pp. 1295–1303, Mar. 2012.
- [6] B. N. Alajmi, K. H. Ahmed, S. J. Finney, and B. W. Williams, "A maximum power point tracking technique for partially shaded photovoltaic systems in microgrids," *IEEE Trans. Ind. Electron.*, vol. 60, no. 4, pp. 1596–1606, Apr. 2013.
- [7] K. Kurokawa, H. Sugiyama, D. Uchida, K. Sakuta, K. Sakamoto, T. Ohshiro, T. Matsuo, and T. Katagiri, "Extended performance analysis of 70 PV systems in Japanese field test program," in *Proc. 26th IEEE Photovoltaic Spec. Conf.*, 1997, pp. 1249–1252.
- [8] Z. Salam and M. Z. Ramli, "A simple circuit to improve the power yield of PV array during partial shading," in *Proc. IEEE Energy Convers. Congr. Expo.*, 2012, pp. 1622–1626.
- [9] R. Kadri, J. P. Gaubert, and G. Champenois, "Non-dissipative string current diverter for solving the cascaded DC–DC converter connection problem in photovoltaic power generation system," *IEEE Trans. Power Electron.*, vol. 27, no. 3, pp. 1249–1258, Mar. 2012.
- [10] K. Ishaque, Z. Salam, and Syafaruddin, "A comprehensive MATLAB simulink PV system simulator with partial shading capability based on two-diode model," *Solar Energy*, vol. 85, pp. 2217–2227, 2011.
- [11] C. R. Sullivan, J. J. Awerbuch, and A. M. Latham, "Decrease in photovoltaic power output from ripple: Simple general calculation and the effect of partial shading," *IEEE Trans. Power Electron.*, vol. 28, no. 2, pp. 740–747, Feb. 2013.
- [12] R. C. N. Pilawa-Podgurski and D. J. Perreault, "Submodule integrated distributed maximum power point tracking for solar photovoltaic applications," *IEEE Trans. Power Electron.*, vol. 28, no. 6, pp. 2957–2967, Jun. 2013.
- [13] K. Ishaque, Z. Salam, M. Amjad, and S. Mekhilef, "An improved particle swarm optimization (PSO) based MPPT for PV with reduced steady-state oscillation," *IEEE Trans. Power Electron.*, vol. 27, no. 8, pp. 3627–3638, Aug. 2012.
- [14] T. Shimizu, O. Hashimoto, and G. Kimura, "A novel high-performance utility-interactive photovoltaic inverter system," *IEEE Trans. Power Electron.*, vol. 18, no. 2, pp. 704–711, Mar. 2003.
- [15] K. Ishaque and Z. Salam, "A review of maximum power point tracking techniques of PV system for uniform insolation and partial shading condition," *Renewable Sustainable Energy Rev.*, vol. 19, pp. 475–488, 2013.
- [16] E. Koutroulis and F. Blaabjerg, "A new technique for tracking the global maximum power point of PV arrays operating under partial-shading conditions," *IEEE J. Photovoltaics*, vol. 2, no. 2, pp. 184–190, Apr. 2012.
- [17] H. Patel and V. Agarwal, "Maximum power point tracking scheme for PV systems operating under partially shaded conditions," *IEEE Trans. Ind. Electron.*, vol. 55, pp. 1689–1698, 2008.
- [18] Z. S. H. Taheri and K. Ishaque, "A novel maximum power point tracking control of photovoltaic system under partial and rapidly fluctuating shadow conditions using differential evolution," in *Proc. 2010 IEEE Symp. Ind. Electron. Appl.*, 2010, pp. 82–87.
- [19] E. Bianconi, J. Calvente, R. Giral, E. Mamarelis, G. Petrone, C. A. Ramos-Paja, G. Spagnuolo, and M. Vitelli, "A fast current-based MPPT technique employing sliding mode control," *IEEE Trans. Ind. Electron.*, vol. 60, no. 3, pp. 1168–1178, Mar. 2013.
- [20] S. Jing Jun and L. Kay-Soon, "Photovoltaic model identification using particle swarm optimization with inverse barrier constraint," *IEEE Trans. Power Electron.*, vol. 27, no. 9, pp. 3975–3983, Sep. 2012.
- [21] A. K. Abdelsalam, A. M. Massoud, S. Ahmed, and P. Enjeti, "High-performance adaptive perturb and observe MPPT technique for photovoltaic-based microgrids," *IEEE Trans. Power Electron.*, vol. 26, no. 4, pp. 1010–1021, Apr. 2011.
- [22] H. Guan-Chyun, I. H. Hung, T. Cheng-Yuan, and W. Chi-Hao, "Photovoltaic power-increment-aided incremental-conductance MPPT with two-phased tracking," *IEEE Trans. Power Electron.*, vol. 28, no. 6, pp. 2895–2911, Jun. 2013.
- [23] K. Ishaque and Z. Salam, "A deterministic particle swarm optimization maximum power point tracker for photovoltaic system under partial shading condition," *IEEE Trans. Ind. Electron.*, vol. 60, no. 8, pp. 3195–3206, Aug. 2013.
- [24] M. Adly and A. H. Besheer, "An optimized fuzzy maximum power point tracker for stand alone photovoltaic systems: Ant colony approach," in *Proc. 2012 7th IEEE Conf. on Ind. Electron. Appl.*, 2012, pp. 113–119.
- [25] N. Tat Luat and L. Kay-Soon, "A global maximum power point tracking scheme employing DIRECT search algorithm for photovoltaic systems," *IEEE Trans. Ind. Electron.*, vol. 57, no. 10, pp. 3456–3467, Oct. 2010.
- [26] C. Huang-Jen, L. Yu-Kang, Y. Chun-Yu, C. Shih-Jen, H. Chi-Ming, C. Ching-Chun, K. Min-Chien, H. Yi-Ming, J. Yuan-Bor, and H. Yung-Cheng, "A module-integrated isolated solar microinverter," *IEEE Trans. Ind. Electron.*, vol. 60, no. 2, pp. 781–788, Feb. 2013.
- [27] Z. Yan, L. Liming, and L. Hui, "A high-performance photovoltaic module-integrated converter (MIC) based on cascaded quasi-z-source inverters (qZSI) using eGaN FETs," *IEEE Trans. Power Electron.*, vol. 28, no. 6, pp. 2727–2738, Jun. 2013.
- [28] G. R. Walker and P. C. Sernia, "Cascaded DC–DC converter connection of photovoltaic modules," *IEEE Trans. Power Electron.*, vol. 19, no. 4, pp. 1130–1139, Jul. 2004.
- [29] L. Duo, Z. Zhe, X. Biwen, C. Min, and Q. Zhaoming, "A method of power decoupling for long life micro-inverter," in *Proc. 37th Annu. Conf. IEEE Ind. Electron. Soc.*, 2011, pp. 802–807.
- [30] R. S. Balog, K. Yingying, and G. Uhrhan, "A photovoltaic module thermal model using observed insolation and meteorological data to support a long life, highly reliable module-integrated inverter design by predicting expected operating temperature," in *Proc. IEEE Energy Convers. Congr. Expo.*, 2009, pp. 3343–3349.
- [31] Z. Qi, S. Xiangdong, Z. Yanru, and M. Mikihiro, "A novel topology for solving the partial shading problem in photovoltaic power generation system," in *Proc. IEEE 6th Int. Power Electron. Motion Control Conf.*, 2009, pp. 2130–2135.
- [32] C. Shih-Ming, L. Tsorng-Juu, Y. Lung-Sheng, and C. Jiann-Fuh, "A safety enhanced, high step-up DC–DC converter for AC photovoltaic module application," *IEEE Trans. Power Electron.*, vol. 27, no. 4, pp. 1809–1817, Apr. 2012.
- [33] Z. Qian, H. Changsheng, C. Lin, A. Amirahmadi, N. Kutkut, Z. J. Shen, and I. Batarseh, "A center point iteration MPPT method with application on the frequency-modulated LLC microinverter," *IEEE Trans. Power Electron.*, vol. 29, no. 3, pp. 1262–1274, Mar. 2014.
- [34] J. Shuai, C. Dong, L. Yuan, and P. Fang-Zheng, "Grid-connected boost-half-bridge photovoltaic microinverter system using repetitive current control and maximum power point tracking," *IEEE Trans. Power Electron.*, vol. 27, no. 11, pp. 4711–4722, Nov. 2012.
- [35] H. J. Bergveld, D. Buthker, C. Castello, T. Doorn, A. de Jong, R. van Otten, and K. de Waal, "Module-level DC/DC conversion for photovoltaic systems: The delta-conversion concept," *IEEE Trans. Power Electron.*, vol. 28, no. 4, pp. 2005–2013, Apr. 2013.
- [36] K. Young-Ho, J. Young-Hyok, K. Jun-Gu, J. Yong-Chae, and W. Chung-Yuen, "A new control strategy for improving weighted efficiency in photovoltaic AC module-type interleaved flyback inverters," *IEEE Trans. on Power Electron.*, vol. 28, no. 6, pp. 2688–2699, Jun. 2013.
- [37] D. R. Nayanasiiri, D. M. Vilathgamuwa, and D. L. Maskell, "Half-wave cycloconverter-based photovoltaic microinverter topology with

- phase-shift power modulation,” *IEEE Trans. Power Electron.*, vol. 28, no. 6, pp. 2700–2710, Jun. 2013.
- [38] G. R. Walker and J. C. Pierce, “Photovoltaic DC–DC module integrated converter for novel cascaded and bypass grid connection topologies; design and optimisation,” in *Proc. 37th IEEE Power Electron. Spec. Conf.*, 2006, pp. 1–7.
- [39] L. F. L. Villa, H. Tien-Phu, J. C. Crebier, and B. Raison, “A power electronics equalizer application for partially shaded photovoltaic modules,” *IEEE Trans. Ind. Electron.*, vol. 60, no. 3, pp. 1179–1190, Mar. 2013.
- [40] I. Abdalla, J. Corda, and L. Zhang, “Multilevel DC-link inverter and control algorithm to overcome the PV partial shading,” *IEEE Trans. Power Electron.*, vol. 28, no. 1, pp. 14–18, Jan. 2013.
- [41] G. Lijun, R. A. Dougal, L. Shengyi, and A. P. Iotova, “Parallel-connected solar PV system to address partial and rapidly fluctuating shadow conditions,” *IEEE Trans. Ind. Electron.*, vol. 56, no. 5, pp. 1548–1556, May 2009.
- [42] K. Ishaque, Z. Salam, and H. Taheri, “Simple, fast and accurate two diode model for photovoltaic modules,” *Solar Energy Mater. Solar Cells*, vol. 95, pp. 586–594, 2011.
- [43] M. A. G. de Brito, L. Galotto, L. P. Sampaio, G. de Azevedo e Melo, and C. A. Canesin, “Evaluation of the Main MPPT techniques for photovoltaic applications,” *IEEE Trans. Ind. Electron.*, vol. 60, no. 3, pp. 1156–1167, Mar. 2013.
- [44] A. Dolara, R. Faranda, and S. Leva, “Energy comparison of seven MPPT techniques for PV systems,” *J. Electromagn. Anal. Appl.*, vol. 3, pp. 152–162, 2009.
- [45] Z. Zhe, Z. Ouyang, O. C. Thomsen, and M. A. E. Andersen, “Analysis and design of a bidirectional isolated DC–DC converter for fuel cells and supercapacitors hybrid system,” *IEEE Trans. Power Electron.*, vol. 27, no. 2, pp. 848–859, Feb. 2012.



Mohd. Zulkiffi Ramli was born in Terengganu, Malaysia in 1978. He received the B.Sc. and M.Eng. degrees from the Universiti Teknologi Malaysia (UTM), Johor Bahru, Malaysia, in 2000 and 2004, respectively, all in electrical engineering. He is currently working toward the Ph.D. degree at UTM in the area of photovoltaic.

He is currently a Senior Lecturer at the Universiti Teknikal Melaka, Melaka, Malaysia. His primary research interests include the hardware design of all power converters and their control systems.



Zainal Salam (M'99) received the B.Sc. degree in electronics engineering from the California State University, Chico, CA, USA, the M.E.E. degree in electrical engineering from the Universiti Teknologi Malaysia (UTM), Johor Bahru, Malaysia, and the Ph.D. degree in power electronics, from the University of Birmingham, Birmingham, U.K., in 1985, 1989, and 1997, respectively.

He has been a Lecturer for 28 years and is currently the Professor in power electronics and renewable energy at the Faculty of Electrical Engineering

UTM. He currently holds the position of *Dean of Research* for Energy Research Alliance—overseeing and managing energy-related research work in the University. He is the Founder, and currently the Director, of the Inverter Quality Control Center, UTM. This facility is responsible to test PV inverters that are to be connected to the local utility grid. Since 2011, he has been the Editor of *IEEE TRANSACTION ON SUSTAINABLE ENERGY* (an IEEE Power and Energy Society publication). He represents the country as the expert for the International Energy Agency (IEA) PV Power Systems Task 13 Working Group, which focuses on the reliability and performance of the PV power system. He is the Vice-Chair of IEEE Power Electronics, Industrial Electronics, and Industry Application Joint Chapter, Malaysia Section (2011–2013), Organizing Chairman for the 5th IEEE International Power Electronics and Drives Systems Conference (2005, Kuala Lumpur), and Coorganizing Chairman for the 2nd IEEE International Power and Electronics and Energy Conference (2008, Johor Bahru). His main research interests include all areas of design, instrumentation, and control of power electronics renewable energy systems.